THE LAS CAMPANAS INFRARED SURVEY: EARLY-TYPE GALAXY PROGENITORS BEYOND $z = 1$

P. J. McCarthy,[1] R. G. Carlberg,[2] H.-W. Chen,[1] R. O. Marzke,[1,3] A. E. Firth,[4] R. S. Ellis,[5] S. E. Persson,[1]
R. G. McMahon,[4] O. Lahav,[4] J. Wilson,[1] P. Martini,[1] R. G. Abraham,[2] C. N. Sabbey,[4] A. Oemler,[1]
D. C. Murphy,[1] R. S. Somerville[4] M. G. Beckett,[1,4] J. R. Lewis,[4] AND C. D. MacKay[4]

ABSTRACT

We have identified a population of faint red galaxies from a 0.62 deg^2 region of the Las Campanas Infrared Survey whose properties are consistent with their being the progenitors of early-type galaxies. The optical and IR colors, number-magnitude relation, and angular clustering together indicate modest evolution and increased star formation rates among the early-type field population at redshifts between 1 and 2. The counts of red galaxies with H magnitudes between 17 and 20 rise with a slope that is much steeper than that of the total H sample. The surface density of red galaxies drops from roughly 3000 deg^{-2} at $H = 20.5$, $I-H > 3$ to ~20 deg^{-2} at $H = 20$, $I-H > 5$. The $V-I$ colors are approximately 1.5 mag bluer on average than a pure old population and span a range of more than 3 mag. The strength of the angular clustering of the red galaxies is an order of magnitude larger than that of the full galaxy sample. The colors, and photometric redshifts derived from them, indicate that the red galaxies have redshift distributions adequately described by Gaussians with $\sigma_z \simeq 0.2$ centered near $z = 1$, with the exception that galaxies having $V-I < 1.6$ and $I-H > 3$ are primarily in the $1.5 \lesssim z \lesssim 2$ range. We invert the angular correlation functions using these $n(z)$ and find comoving correlation lengths of $r_0 \simeq 9$–$10\ h^{-1}$ Mpc at $z \simeq 1$, comparable to, or larger than, those found for early-type galaxies at lower redshifts. A simple photometric evolution model reproduces the counts of the red galaxies, with only an ~30% decline in the underlying space density of early-type galaxies at $z \sim 1.2$. The colors indicate characteristic star formation rates of ~1 $M_\odot$ yr^{-1} per $10^{10}\ M_\odot$. We suggest on the basis of the colors, counts, and clustering that these red galaxies are the bulk of the progenitors of present-day early-type galaxies.

Subject headings: galaxies: evolution — galaxies: high-redshift — surveys

1. INTRODUCTION

The earliest deep images at high latitude obtained with near-IR arrays revealed a population of galaxies not represented in optical surveys (e.g., Elston, Rieke, & Rieke 1988; McCarthy, Persson, & West 1992; Hu & Ridgway 1994). These objects have colors and apparent magnitudes close to those expected of evolved massive galaxies at $1 < z < 3$. Selections based on $R-K$ lead to a heterogeneous population containing evolved stellar populations (Spinrad et al. 1997; Soifer et al. 1999), reddened objects (Graham & Dey 1996; Cimatti et al. 1998; Dey et al. 1999; Barger, Cowie, & Richards 2000), and cool stars. Redshifts for either dust-free or highly reddened objects are primarily in the $1 < z < 2$ range (Graham & Dey 1996; Soifer et al. 1999; Liu et al. 2000; Cowie et al. 2001). While the reddest examples (Smail et al. 1999) are sometimes associated with bright submillimeter sources and centimeter-wave sources, the bulk of the red galaxies do not appear to be strong centimeter-to-submillimeter continuum sources.

A key issue in the hierarchical assembly picture of galaxy formation is the identification of the redshift range over which the most massive galaxies assemble. The effects of merging at $z < 1$ are minor: the luminosity function evolves primarily through passive evolution (Lilly et al. 1995; Cowie et al. 1996), and the merger rate is low (Carlberg et al. 2000). The rate of mass buildup via merging is dependent on the density of gal-

axies, the correlation function at relevant separations, and the distribution of pairwise velocities. For major mergers to play a dominant role in galaxy building, the clustering of at least some component of the normal galaxy population must be large relative to that at the current epoch. Near-IR selection provides a powerful tool for removing the foreground of faint low-redshift star-forming galaxies and offers a path toward selecting galaxies at $z \sim 1$ by stellar mass.

The Las Campanas Infrared (LCIR) Survey was crafted to select early-type galaxies at $1 < z < 2$ (Marzke et al. 1999). It is a near-IR survey to $H \sim 21$ over a significant fraction of a square degree, supplemented by photometry in the $UBVRIz'$ bands. In this Letter, we present the basic observational results for the galaxy counts, colors, and clustering properties along with their implications based on simple modeling. Future papers will augment these data and refine and broaden the interpretation.

2. OBSERVATIONS AND RESULTS

2.1. *Observations*

The data presented here are drawn from a subset of the LCIR Survey covering an area of 0.62 deg^2 to a depth ranging from $H = 20$ to 21 in four fields: the Hubble Deep Field–South (HDF-S), the Chandra Deep Field–South (CDF-S), SSA22, and the New Technology Telescope (NTT) Deep Field. The H data, obtained with the Cambridge Infrared Survey Instrument (CIRSI) camera (Beckett et al. 1998), are complemented by deep optical imaging: VRI in all fields, U and B in HDF-S, and z' in CDF-S. The details of the near-IR survey are described in Chen et al. (2001) and Firth et al. (2001), while the optical data are discussed in R. O. Marzke et al. (2001, in preparation).

[1] Carnegie Observatories, 813 Santa Barbara Street, Pasadena, CA 91101.
[2] Department of Astronomy, University of Toronto, 60 St. George Street, Toronto, ON M5S 3H8, Canada.
[3] Department of Astronomy and Physics, San Francisco State University, San Francisco, CA 94132.
[4] Institute of Astronomy, Madingley Road, Cambridge CB3 OHA, UK.
[5] Department of Astronomy, California Institute of Technology, MS 105-24, Pasadena, CA 91125.
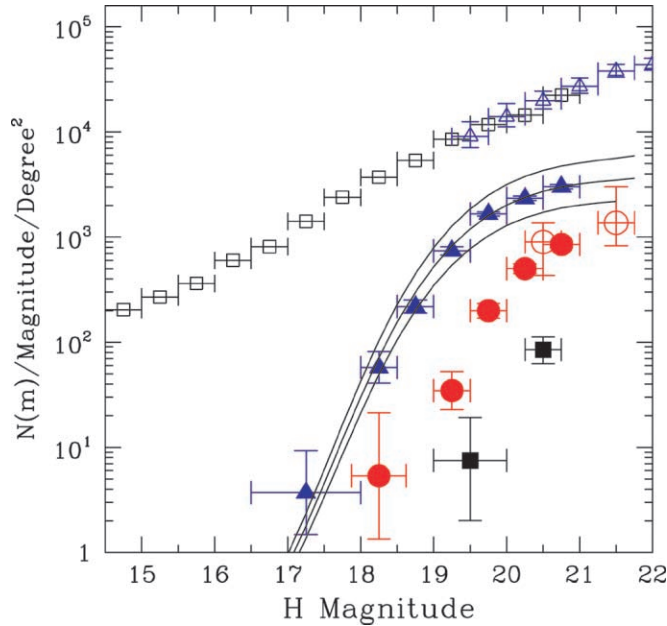
FIG. 1.—Total and red galaxy counts as a function of H magnitude over 0.62 deg^2 in four fields. The open squares represent the complete galaxy sample, after removal of stars. The open triangles are the NICMOS-based H counts from Yan et al. (1998). The filled triangles and circles are the H counts for $I-H > 3$ and 4, respectively. The error bars show the 95% confidence interval assuming Poisson statistics. The open circles at $H = 20.5$ and 21.5 are from the $R-H > 5$ NICMOS sample of Yan et al. (2000). The filled squares are the counts for $I-H > 5$ from the CDF-S and HDF-S fields only. The curves show the counts for $I-H > 3$ derived from the evolving population models described in the text with $p = 0$, 0.5, and 1. The characteristic redshift for the $I-H > 3$ model is 1.2.

Photometric catalogs were extracted for each field using 4″ aperture Johnson magnitudes.

2.2. N(m) for Red Galaxies

In Figure 1, we present the differential number magnitude relations for the complete H-selected sample and $I-H$ color-selected subsamples from the HDF-S, CDF-S, SSA22, and NTT fields. These counts are based on 4″ aperture magnitudes with aperture and incompleteness corrections derived from point sources. Each field was used only to its 95% completeness limit. A full analysis of the number counts and their completeness are given in Chen et al. (2001) and Firth et al. (2001). The complete H counts are similar in slope, $d \log n/dm$, and amplitude to the deep H counts derived by Yan et al. (1998). The $I-H > 3$ counts are quite steep, $d \log n/dm = 1.1$ in the $17 < H < 19.5$ range. At fainter levels, the counts must flatten, and the slope of the $I-H > 3$ subsample appears to change near $H = 19.5$. The counts in the redder color bin appear to have the same slope as the $I-H > 3$ counts for $H < 20$ but with surface densities that fall roughly 1 order of magnitude per magnitude of increasingly red color. At bright magnitudes (e.g., $H \sim 17.5$), the red galaxies constitute roughly 0.5% of the total H-selected population with a surface density of a few per square degree, while at $H = 20.5$ they contribute roughly 10% of the total population at a density of ~3000 deg^{-2}. We note that our primary color cut, $I-H > 3$, is roughly 1 mag bluer than the canonical "extremely red object" color threshold of $R-K > 6$.

We use a set of simple evolutionary models to examine both the red counts and the colors (§ 2.3), computed with the PEGASE.2 code (Fioc & Rocca-Volmerange 1997) and the Gardner et al. (1997) local K-band luminosity function. We
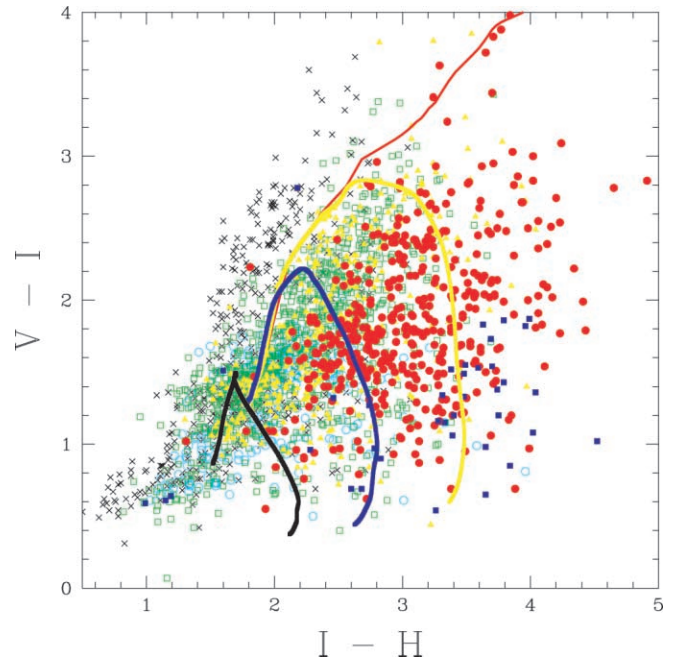

FIG. 2.—The $V-I$ vs. $I-H$ colors for objects with $19 < H < 20.5$ in the CDF-S field. The points are color-coded on the basis of their photometric redshift: stars (*black crosses*), $z < 0.25$ (*cyan open circles*), $0.25 < z < 0.75$ (*green open squares*), $0.75 < z < 1.0$ (*yellow filled triangles*), $1 < z < 1.5$ (*red filled circles*), and $1.5 < z < 2.0$ (*blue filled squares*). The model curves show the loci of evolving population models with various star formation laws: a single burst with $z_f = 30$ (*red curve*), exponential decline with $\tau = 1$ and 2 Gyr (*yellow and blue curves*), and continuous (*black curve*). The yellow curve is from the same model used in Figure 1.

identify the red galaxy population as those galaxies brighter than $M_* - 1$ as fitted with a Schechter function with $\alpha = 1$ and $M_*(\text{red}) = M_* - 0.2$ and $\phi_*(\text{red}) = 0.15\phi_*$. Assuming the $I-H$ colors at the faint limit of our sample have a precision of 0.25 mag, this model luminosity function is evolved using a $\tau = 1$ decaying star formation rate model and a number density that evolves as $(1 + z)^{-p}$ in an $\Omega_M = 0.3$, $\Omega_\Lambda = 0.7$ cosmology to predict the red galaxy number counts in Figure 1. Density evolution with $p = 0.5 \pm 0.2$ agrees well with the observed counts of galaxies with $I-H > 3$ and implies a decline in true space density of ~30% at $z = 1.2$.

There have been a variety of measurements of the surface density of red objects from near-IR surveys, primarily based on $R-K$ selected samples. At the faint end, our surface density of 1000 deg^{-2} for $I-H > 4$ agrees well with the Near-Infrared Camera and Multi-Object Spectrometer (NICMOS) measurements reported by Yan et al. (2000) for $R-H > 5$. Our counts at $H = 20$, $I-H > 4$ agree well with the surface density of 150 deg^{-2} for $R-K > 6$, $K < 19.0$ reported by Thompson et al. (1999), and our counts at $I-H > 3$ agree with those reported by Daddi et al. (2000) for $R-K > 5$.

2.3. Optical and Near-IR Colors

Stars and galaxies at different redshifts have distinctive signatures in an optical near-IR color-color diagram. In Figure 2, we plot the $V-I$ versus $I-H$ diagram from the CDF-S field for $19 \le H \le 20.5$. The points are color-coded on the basis of photometric redshifts (H.-W. Chen et al. 2001, in preparation; Firth et al. 2001). The red galaxies with $I-H > 3$ span more than 3 mag in $V-I$. This wide range of optical colors worked against previous searches for early-type galaxies at $z > 1$ that
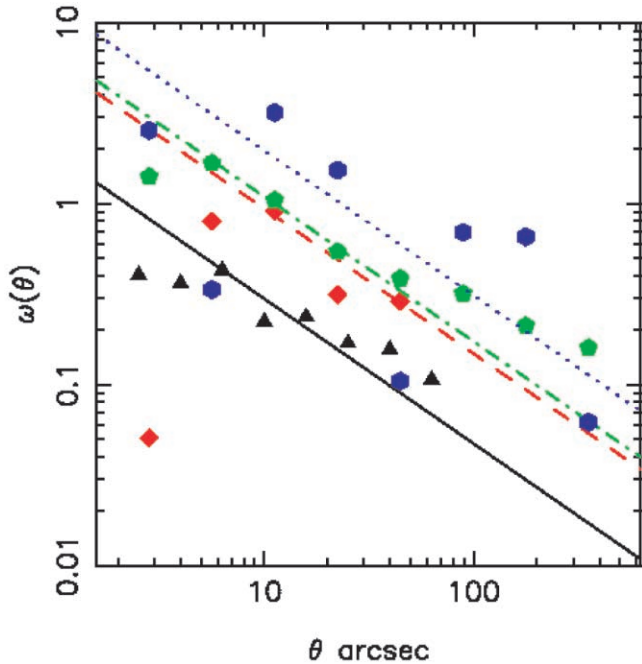
FIG. 3.—Angular correlation function for various color and magnitude sub-samples: all colors for $19 < H < 20.5$ (*black triangles*) and $I-H > 3$ samples with $18 \leq H \leq 19$ (*blue circles*), $19 \leq H \leq 20$ (*green pentagons*), and $20 \leq H \leq 20.5$ (*red diamonds*). The strong increase with increasing brightness is primarily the result of a narrowing redshift distribution. In all cases, $r_0 \sim 9\ h^{-1}$ Mpc.

TABLE 1
CLUSTERING PROPERTIES OF RED GALAXIES

SUBSAMPLE		θ_0			r_0
H	$I-H$	(arcsec)	$\langle z \rangle$	σ_z	(h^{-1} Mpc)
20.0–20.5	3.0–5.0	5.0 ± 0.2	1.2	0.30	8.4
19.0–20.0	3.0–5.0	15.0 ± 1.0	1.2	0.15	9.5
18.0–19.0	3.0–5.0	50.0 ± 7.0	0.9	0.07	10.7
20.0–20.5	All	2.0 ± 0.2	0.7	0.30	5.7
19.0–20.5	3.0–5.0	6.7 ± 0.4	1.2	0.30	9.8
19.0–20.5	3.5–5.0	6.3 ± 0.5	1.2	0.30	9.5
19.0–20.5	4.0–5.0	11 ± 0.5	1.2	0.20	9.7
19.0–20.5[a]	3.0–5.0	15 ± 2	1.2	0.15	9.6
19.0–20.5[b]	3.0–5.0	12 ± 1	1.6	0.2	9.8

[a] $V-I > 1.8$.
[b] $V-I < 1.8$.

H depth of 20.5, The HDF-S field covers 847 arcmin^2 to an average 90% completeness depth of 20.1. We use the Landy & Szalay (1993) algorithm for estimating $\omega(\theta)$. Uncertainties are computed from the differences between the two fields. We use the population of stars and faint blue galaxies as the random distribution. As a check, we determined $\omega(\theta)$ for a complete H-selected sample using a generated random sample and a completeness map for a subregion of the HDF-S field and recover a clustering angle of approximately 2″.

In Figure 3, we display the angular correlation function for the full H-selected population and for the red galaxies in three apparent magnitude bins, $18 < H < 19$, $19 < H < 20$, and $20 < H < 20.5$. The correlation angles, θ_0, derived from fits to $\omega(\theta) = (\theta_0/\theta)^{\gamma-1}$ ($\gamma = 1.8$ is assumed), are given in Table 1. The clustering shows very steep color and magnitude dependencies, allowing a strong test of the estimated redshift distribution and the spatial correlation length. There are two primary trends: the red galaxies are very much more correlated than the entire H-limited sample, and the angular clustering increases much faster with decreasing limiting magnitude than can be expected on the basis of depth in a uniformly distributed population. The natural interpretation is that the red galaxies are distributed in a relatively narrow redshift shell around $z = 1$. In Table 1, we report the dependence of clustering on color in various subsamples and find that the clustering increases for progressively redder subsamples. We split the $I-H > 3$ galaxies into subsamples with red and blue rest-frame UV colors at $V-I = 1.8$, finding that both subsamples have increased correlations compared to the whole and hence occupy narrower redshift ranges.

required colors that matched purely passive models. It is particularly notable that very few of the red galaxies have $V-I \sim 3$, the color expected of purely old stellar populations. Our estimated 50% completeness limit in V is slightly beyond 26 mag, so we should be missing very few of these inactive red galaxies. Few such objects are seen in deeper fields (e.g., Moustakas et al. 1997). We note that our survey area is such that we sample only the field population and expect to detect few, if any, rich clusters.

Superposed on the data in Figure 2 are the loci of four evolutionary models spanning the $0 < z < 2$ range computed using the PEGASE.2 code (Fioc & Rocca-Volmerange 1997). Note that virtually all objects to the left of the models are stars. With increasing redshift, the colors initially become redder, but as the V band begins to sample the rest-UV part of the spectrum beyond $z = 1$, it begins to brighten. The model that best matches the red galaxy population, an exponentially declining star formation rate with $\tau = 1$ Gyr, is the same model that reproduces the red counts shown in Figure 1. At the redshift of observation, the star formation rates are not insignificant, the rate being $\sim 1\ M_\odot$ yr^{-1} per $10^{10}\ M_\odot$, comparable to the star formation rates in the general field galaxy population at comparable redshifts. The $(I-H)$–defined red galaxies with the bluest $V-I$ colors are expected to lie at $1.5 < z < 2$ on the basis of this model. The photometric redshifts support this, as shown by the significant number of $z_{\rm ph} > 1.5$ objects in the lower right portion of the color-color plane.

2.4. Angular Clustering

We have computed the angular correlation function of the red objects in our fields. The deepest and most complete data sets come from the HDF-S and CDF-S survey areas. The CDF-S field covers 561 arcmin^2 with an average 90% completeness

2.5. Spatial Clustering

The red galaxy counts, colors, and angular clustering together allow us to infer their statistical distribution in redshift. Here we present a simple population model approach using the evolving luminosity function as described in § 2.2.

To invert the θ_0 into comoving correlation length, $r_0(z)$, we use the relativistic generalization of Limber's equation for $\xi(r, z) = [r_0(z)/r]^\gamma$,

$$\omega(\theta) = A(\gamma)\theta^{1-\gamma}N^{-2} \int n^2(z)r_0^\gamma(z)x^{1-\gamma}\frac{H(z)}{c}\ dz, \quad (1)$$

where $N = \int n(z)dz$, $A(\gamma) = \Gamma\left(\frac{1}{2}\right)\Gamma[(\gamma-1)/2]/\Gamma(\gamma/2)$, and $H(z) = H_0[\Omega_M(1 + z)^3 + \Omega_R(1 + z)^2 + \Omega_\Lambda]^{1/2}$, with $\Omega_M + \Omega_R + \Omega_\Lambda = 1$. The comoving distance, $x(z)$, is computed for our adopted cosmology, $\Omega_M = 0.3$, $\Omega_\Lambda = 0.7$.

We approximate the $n(z)$ distributions with Gaussian fits to the results of the population model discussed in § 2.2 (see Table 1). Determinations of $n(z)$ from our photometric redshifts in the CDF-S field yield mean redshifts and characteristic widths for the $I-H > 3$ and $I-H > 3.5$ subsamples quite close to those listed in Table 1. An additional constraint comes from redshifts for objects in similar color and magnitude ranges from the Caltech Faint Galaxy Redshift Survey (Cohen et al. 2000). The Cohen et al. sample is K-selected, but if we adopt $H-K = 1$ for the red population, we can compare the redshift distribution of their $K = 20$ sample. A red color cut yields $\langle z \rangle = 1.2$, $\sigma_z \sim 0.15$, a distribution somewhat narrower than that derived from the photometric redshifts, as expected. We use our population model to mitigate the small number statistics in the photometric redshifts, particularly for the reddest colors and brightest magnitudes. We adopt $\langle z \rangle = 1.2$ for the red galaxies, 0.9 for the $18 \leq H \leq 19$ range, and 1.6 for the $V-I < 1.8$ blue subsample of the $I-H$ red galaxies.

The inferred comoving correlation lengths, r_0, are listed in Table 1. The correlation lengths increase as $\sigma_z^{0.55}$ and have only a very weak dependence on the mean redshift. Although these correlation lengths are large, they are comparable to those found for early-type galaxy populations at low redshifts (Davis & Geller 1976; Guzzo et al. 1997; Willmer, da Costa, & Pellegrini 1998). Our larger inferred values of r_0 at high redshift compared to local early types could be the result of an increasing biasing with redshift, as expected theoretically (Mo & White 1996),

or simply an overestimate of the width of the redshift distribution.

3. CONCLUSIONS

We have identified a large sample of faint red galaxies from a 0.62 deg^2 area of the LCIR Survey. While the present data set does not allow a direct constraint on the contribution from heavily reddening star-forming galaxies, the counts, colors, and clustering statistics of these galaxies are all consistent with their being a mildly evolved progenitor of the present-day early-type field population. We find evidence for a modest change in the comoving space density of early-type galaxies to $z \sim 1.2$. The star formation rates inferred from the rest-frame UV colors suggest that the objects are largely, but not completely, assembled by the epoch of observation. If the red galaxies are predominantly old stellar systems, their numbers are larger than predicted in galaxy evolution models with strong merging (e.g., Kauffmann & Charlot 1998; Somerville, Primack, & Faber 2001). The use of a color selection that does not extend to the rest-frame UV allows us to recognize nearly passively evolving objects with greater confidence than selections spanning large color baselines.

REFERENCES

Barger, A. J., Cowie, L. L., & Richards, E. A. 2000, AJ, 119, 2092
Beckett, M. G., MacKay, C. D., McMahon, R. G., Parry, I. R., Ellis, R. S., Chan, S. J., & Hoenig, M. 1998, Proc. SPIE, 3354, 431
Carlberg, R. G., et al. 2000, ApJ, 532, L1
Chen, H.-W., et al. 2001, ApJ, submitted (astro-ph/0108171)
Cimatti, A., Andreani, P., Rottgering, H., & Tilanus, R. 1998, Nature, 392, 895
Cohen, J. G., Hogg, D. W., Blandford, R., Cowie, L. L., Hu, E., Songaila, A., Shopbell, P., & Richberg, K. 2000, ApJ, 538, 29
Cowie, L. L., Songaila, A., Hu, E. M., & Cohen, J. G. 1996, AJ, 112, 839
Cowie, L. L., et al. 2001, ApJ, 551, L9
Daddi, E., Cimatti, A., Pozzetti, L., Hoekstra, H., Rottgering, H., Renzini, A., Zamorani, G., & Manucci, F. 2000, A&A, 361, 535
Davis, M., & Geller, M. J. 1976, ApJ, 208, 13
Dey, A., Graham, J. R., Ivison, R. J., Smail, I., Wright, G. S., & Liu, M. C. 1999, ApJ, 519, 610
Elston, R., Rieke, G. H., & Rieke, M. J. 1988, ApJ, 331, L77
Fioc, M., & Rocca-Volmerange, B. 1997, A&A, 326, 950
Firth, A. E., et al. 2001, MNRAS, submitted (astro-ph/0108182)
Gardner, J., Sharples, R. M., Frenk, C. S., & Carrasco, B. E. 1997, ApJ, 480, L99
Graham, J. R., & Dey, A. 1996, ApJ, 471, 720
Guzzo, L., Strauss, M. A., Fisher, K. B., Giovanelli, R., & Haynes, M. P. 1997, ApJ, 489, 37
Hu, E. M., & Ridgway, S. E. 1994, AJ, 107, 1303
Kauffmann, G., & Charlot, S. 1998, MNRAS, 297, L23

Landy, S. D., & Szalay, A. S. 1993, ApJ, 412, 64
Lilly, S. J., Tresse, L., Hammer, F., Crampton, D., & Le Fèvre, O. 1995, ApJ, 455, 108
Liu, M. C., Dey, A., Graham, J., Bundy, K., Steidel, C., Adelberger, K., & Dickinson, M. 2000, AJ, 119, 2556
Marzke, R. O., et al. 1999, in ASP Conf. Ser. 191, Photometric Redshifts and the Detection of High Redshift Galaxies, ed. R. Weymann, L. Storrie-Lombardi, M. Sawicki, & R. Brunner (San Francisco: ASP), 148
McCarthy, P. J., Persson, S. E., & West, S. C. 1992, ApJ, 386, 52
Mo, H. J., & White, S. D. M. 1996, MNRAS, 282, 347
Moustakas, L., Davis, M., Graham, J., Peterson, B., & Silk, J. 1997, ApJ, 475, 445
Smail, I., Ivison, R. J., Kneib, J.-P., Barger, A., Owen, F., & Morisson, G. 1999, MNRAS, 308, 1061
Soifer, B. T., Matthews, K., Neugebauer, G., Armus, L., Cohen, J. G., Persson, S. E., & Smail, I. 1999, AJ, 118, 2065
Somerville, R. S., Primack, J. R., & Faber, S. M. 2001, MNRAS, 320, 504
Spinrad, H., Dey, A., Stern, D., Dunlop, J., Peacock, J., Jimenez, R., & Windhorst, R. 1997, ApJ, 484, 581
Thompson, D., et al. 1999, ApJ, 523, 100
Willmer, C. N. A., da Costa, L. N., & Pellegrini, P. S. 1998, AJ, 115, 869
Yan, L., McCarthy, P., Storrie-Lombardi, L., & Weymann, R. J. 1998, ApJ, 503, L19
Yan, L., McCarthy, P., Weymann, R., Malkan, M., Teplitz, H., Storrie-Lombardi, L., Smith, M., & Dressler, A. 2000, AJ, 120, 575